Final Draft
of the original manuscript:

Bohlen, J.; Nuernberg, M.; Senn, J.W.; Letzig, D.; Agnew, S.R:
The Texture and Anisotropy of Magnesium-Zinc-Rare Earth Alloy Sheets
In: Acta Materialia (2007) Elsevier

DOI: 10.1016/j.actamat.2006.11.013

The Texture and Anisotropy of Magnesium-Zinc-Rare Earth Alloy Sheets

Jan Bohlen[1*], Marcus R. Nürnberg[1], Jeremy Senn[2], Dietmar Letzig[1], and Sean R. Agnew[2*]

[1]GKSS Forschungszentrum, Magnesium Innovation Centre (MAGIC), Max Planck Str. 1, D-21502 Geesthacht, Germany

[2]University of Virginia, Charlottesville, Virginia, 22904-4745

Abstract

In this paper, the rolling textures of six magnesium alloys containing different levels of zinc and rare earth (e.g., mischmetal or Y) additions are examined. The overall texture strength and the basal pole intensity aligned with the sheet normal direction is lower for rare earth containing alloys than for conventional alloys. The distinct textures generated in this study allow investigation of the influence of texture on the mechanical response. The anisotropy of the yield and flow strengths is reversed and the planar anisotropy is reduced ($r \sim 1$) in comparison to conventional alloys. Both aspects of the anisotropy are related to the fact that the dominant texture components in the Mg-Zn-RE alloys place more grains in favourable orientations for basal slip and tensile twinning, particularly during transverse direction tension. Mg sheets with lower r-value promise to have improved forming behaviour, at least under straining conditions which call for thinning of the sheet.

Keywords: magnesium, crystal plasticity, solid solution, recrystallization, mischmetal, cerium, yttrium

*Corresponding authors:

Dr. Jan Bohlen, email: jan.bohlen@gkss.de

Dr. Sean Agnew, Assist. Prof, email: agnew@virginia.edu

Introduction

Improving fuel efficiency and reducing emissions of vehicles can be achieved through light weight construction. Magnesium and its alloys offer a remarkable potential in this regard as the lightest construction metals [1]. Unfortunately, present magnesium wrought alloys are limited in their formability. A possible contributor to the formability problem is the strong crystallographic texture which is typical of magnesium sheets. The vast majority of grains are oriented such that their basal (00.1) planes are close to the sheet plane. Due to the intrinsic plastic anisotropy of the hexagonal close packed crystals, such a texture places most grains in an orientation where it is difficult to deform, resulting in high flow stresses, modest work hardening and, therefore, low values of uniform elongation. Magnesium alloy polycrystals with more random textures result in higher strain hardening rates [2] than commonly observed in typically textured wrought products [3]. Such improved strain hardening behaviour promotes stable plastic flow necessary for improved formability [4]. Additionally, such textured materials have a strong tension-compression strength asymmetry associated with the polar nature of mechanical twinning, which results in strange bending characteristics, such as failure initiation on the compression side of bent sheets [5] and tubes [6].

The potential to improve the formability of magnesium alloys by modifying the texture has been demonstrated [7]. Thin sheets were sectioned from a thick plate with a texture gradient and it was found that the sections with the weaker (more random) texture exhibited the highest formability. However, the strong basal texture and resulting mechanical properties have appeared to be essentially inevitable within the range of typical industrial wrought processing techniques used to produce sheets, although a wide range of wrought magnesium alloy compositions and sheet processing schemes have been explored in the past.

It has recently been observed that alloys containing additions of yttrium (Y) and rare earth (RE) elements such as neodymium (Nd) can develop more random textures during hot extrusion [8] and during plane strain compression followed by annealing [9]. The deformation

texture of these alloys is not very distinct from other magnesium alloys, rather recrystallization appears to strongly alter the texture. The randomized texture has been associated with particle stimulated nucleation (PSN) of recrystallization (RXX) [8, 10, 11]. PSN has been cited as a texture randomizing mechanism which is exploited in the production of other metals, such as aluminium alloys [12]. Indeed, the alloys examined previously did have high alloying contents, such that precipitation is expected and PSN becomes an attractive explanation for the observed texture randomization. The ability to randomize the texture of wrought magnesium alloys has positive implications, such as reducing the tension/compression strength asymmetry as well as the potential to improve the secondary formability mentioned above. However, the alloys in which the effect has been observed were originally developed for high strength and creep resistance and are unsuitable for sheet processing.

This paper reports on a study of magnesium alloys with only dilute additions of RE or Y, which are more appropriate for sheet processing (< 1 wt%). All the different alloys examined contain zinc as the main alloying element in the range of 1 – 4 wt.%. The effect of alloying additions on the resulting sheet texture will be examined. These textures will then be correlated to the mechanical response of sheets, especially in terms of the in-plane yield stress and strain (r-value) anisotropy, as well as the uniform elongation as indicators of sheet formability.

Experimental

Six sheet alloys were examined in the present study. Five of them were processed on industrial scale and examined in an as-rolled (hot-rolled) condition. These alloys are ZK10, ZE10, its modification with zirconium ZEK100, an alloy with higher zinc content ZEK410, as well as a similar alloy containing yttrium ZW41. The chemical compositions of these alloys are listed in Table 1. One further alloy, which is representative of “conventional” wrought

magnesium alloys, ZM21 was cast and machined into slabs for rolling experiments in the laboratory. The sample geometry was 240 mm x 70 mm x 7.4 mm. A homogenization heat treatment was conducted for 16 hr at 400°C prior to rolling. The rolling procedure consisted of 6 passes with a constant reduction of thickness each referring to a true strain

$$\varphi = -\ln\left(h_{n+1}/h_n\right) = 0.3\,, \tag{1}$$

where n is the number of the pass and h_n is the sample thickness after pass n. After every pass, the sheet was re-heated to 400°C for 15 minutes to keep the rolling temperature consistent.

The final gage of all samples examined in this study was 1.0 – 1.4 mm thickness (Table 1). The ZM21 sheet at final gauge received a heat treatment for 0.5 hr. at 400°C. Similarly, the heavily twinned microstructure of alloy ZK10 in the as-rolled condition was suggestive of being rolled at lower temperatures during final rolling steps. Thus, it too received a partial recrystallization heat treatment of 1 hr at 300ºC in order to produce a microstructure comparable to that observed in the other alloys. (This had little impact on the observed texture, though the strength values were reduced and the ductility values increased.)

Universal testing machines were used for tensile testing at room temperature with a constant strain rate of 10^{-3} or 5 x 10^{-3} s^{-1} (strain rate sensitivity studies have shown such Mg alloys to be rate insensitive at room temperature [3, 13].) Samples were taken in three sample orientations from sheets – rolling direction (RD), 45° and transverse direction (TD). Extensometers were used to simultaneously measure changes in length and width during many of the tests. In other cases, the changes in width were measured ex-situ on samples for which the tests were interrupted at a strain of $\varphi \sim 0.09$. R-values were calculated in each sample orientation as

$$r = \varphi_w / \varphi_t = -\varphi_w /\left(\varphi_l + \varphi_w\right), \tag{2}$$

where φ is the true plastic strain along the sample length l, width w, and thickness t.

To analyse the microstructure by optical microscopy, standard metallographic sample preparation techniques were employed including the use of an etchant based upon picric acid [14] which revealed the grains and grain boundaries. The average grain size was determined from several micrographs from longitudinal sections using a computer-aided linear intercept measurement. A scanning electron microscope (SEM), ZEISS DSM 962 was used with an accelerating voltage of 20 keV to perform chemical analysis of second phase particles using energy dispersive X-ray spectroscopy (EDS).

Samples were cut from sheets, ground to their mid-planes, and heavily etched for texture measurements. A Scintag X1 X-ray diffractometer using Cu K_α radiation and equipped with a four-circle goniometer was applied in reflection geometry. The (00.2), (10.0) and (11.0) pole figures were measured to a sample tilt of 80°. Experimental defocusing correction and calculation of the complete orientation distribution, allows recalculation and presentation of complete pole figures.

Results

Microstructure

Sample micrographs from the longitudinal sections of the sheets are shown in Fig. 1. Partially recrystallized microstructures with twins and shear bands are observed as a result of the deformation history of the sheets. The average grain size is summarized in Table 1. There is no substantial difference in the average grain size in ZM21 and ZE10 varying in the range of 18 – 22 μm. Alloys ZK10, ZEK100, and ZEK410, which contain zirconium as a grain refiner, have finer microstructures with a grain size of 9-10 μm. Alloy ZW41, with high Zn additions, has an intermediate grain size of 15 μm.

The microstructures contain varying amount of precipitates with different composition. With increasing alloy content, an increasing number of particles are observed, see Fig. 2 and Table 2. EDS analysis of alloy ZM21 shows precipitates consist of Zn, Mn and Mg. There are

actually very few precipitates in ZK10, which typically appear to contain Zn, Zr, and Mg. These particles are small relative to the interaction volume of the electron probe, thus the magnesium content of the particles may be over-estimated.The rare earth containing alloys all have precipitates containing Zn and RE elements. For example, ZE10 contains precipitates consisting of Zn, Ce and La. If the alloy contains zirconium, e.g., ZEK100 and ZEK410, some particles are found that consist of Zn and Zr. Finally, alloy ZW41 contains precipitates with Zn and Y. There is no visible tendency for precipitates to lie on grain boundaries. However, precipitates are sometimes arranged in "stringers," especially in ZE10 and ZW41, but all single particles are of a globular type.

Texture

Figure 3 shows recalculated (00.2) and (10.0) pole figures of the sheets. There is a tendency to exhibit a "basal" texture in which the majority of grains are oriented such that their (00.1) basal planes are close to the plane of the sheet. However, there are strong variations in the intensity of this basal texture and the exact orientation of the highest intensity region within the basal pole figures varies significantly. In most cases, the peak intensity is tilted slightly away from the sheet normal direction (ND) toward the rolling direction (RD). This is clearly illustrated in Figure 4 where the intensities in the basal pole figure are presented as a function of tilt from the ND toward the RD and transverse (TD) directions. Alloy ZM21 (with no RE/Y) has a strong basal texture, with a peak intensity in the basal pole figure of > 8 multiples of a random distribution (M.R.D.) and an angular distribution that is slightly broader toward the RD than the TD. There is a symmetrical splitting of the peaks in intensity by ± 10° from the ND toward the RD. This texture is typical of conventional magnesium alloy sheets, such as AZ31B (nominally Mg-3 Al-1 Zn-0.3 Mn) [15]. The corresponding prismatic planes (10.0) are therefore oriented perpendicular to the sheet plane, but with no distinctive preferred orientation of the (10.0) poles within the plane of the sheet.

All the rest of the zinc containing alloys examined in this study have lower basal pole intensity parallel to the sheet ND and the highest intensity point is more tilted (± 20°) away from the ND toward the RD. For example, Figure 4 shows that alloy ZK10 has a similarly strong texture as ZM21, but the orientation of the components is distinct. As discussed below, the addition of Mn to Mg-Zn alloys suppresses the Zn solubility [16]. Therefore, it is hypothesized that the reason the ZM21 has a distinct texture from the rest of the alloys is the lower Zn solute content.

This texture description of alloy ZK10 also holds for the rare earth containing alloys, such as ZE10 and ZEK100. In fact, the texture of these two sheets is approximately the same, which suggests that the grain refining zirconium additions to ZEK100 do not strongly affect the deformation and recrystallization mechanisms responsible for texture evolution.. However, the addition of rare earth elements does produce a number of qualitative changes relative to the texture observed in ZK10 (see Figs. 3 & 4).

i) The textures are weaker overall, as indicated by the lower peak intensities.

ii) The angular distribution of basal poles is significantly broader toward the TD whereas the overall spread toward the RD is not significantly affected.

iii) While the poles of the (10.0) prismatic planes tend to lie close to the sheet plane, they are preferentially oriented parallel to the RD.

The higher zinc content alloys, ZEK410 and ZW41, exhibit the same three qualitative features as described for ZE10 and ZEK100, though to an even greater extent. It is noted that the different rare earth alloying elements, yttrium in ZW41 and mainly cerium in ZEK410, have a very similar effect on the texture.

Mechanical properties

Typical stress – strain curves from tensile tests are shown in Figure 5 for RD, 45° and TD. Related mechanical properties are summarized in Table 3. Alloy ZM21 exhibits a yield

anisotropy typical of conventional magnesium alloys, such as AZ31B [16]. The highest yield strength is measured along the TD and the lowest along the RD. Additionally, the yield point is much more pronounced in the TD than in any other orientation. The elongation–to–failure is slightly higher in RD than in other orientations. The strain hardening behavior is rather low and similar along the different directions. Finally, the planar anisotropy, or r-value, (determined at 8% strain) is lowest along the RD and increases toward TD. The average r-value,

$$r_{avg} = \tfrac{1}{4}\left(r_{RD} + 2r_{45} + r_{TD}\right), \tag{3}$$

is significantly greater than 1 (i.e., the sheet material resists thinning during in-plane tensile deformation.).

In comparison to this typical behavior of magnesium alloy sheets [e.g., 16], the results obtained from the rare earth containing alloys are in many ways opposite. The yield strength is highest in the RD and decreases towards the TD. The elongation–to–failure is lowest along the RD. It is noteworthy that there is a large difference between the behavior of the RD and 45° oriented samples, whereas the differences between the 45° and TD samples are less significant. The strain hardening behavior along different directions is quite distinct. The alloys exhibit rather low strain hardening rates along the RD, similar to those observed in alloy ZM21. Along the TD, the hardening rates are significantly higher and the shape of the flow curves approaches linear hardening during the first few percent strain. Finally, the r-values for all the directions are close to 1, as are the average r-values (see Eq. 3 and Table 4). This tendency towards isotropy promises to improve the sheet formability under some forming conditions.

As was observed for the texture results above, the mechanical property trends observed for alloy ZK10 are intermediate to those of ZM21 and the RE/Y containing alloys. The flow strengths are essentially isotropic, while the ductility is highest for the 45° oriented samples and the RD and TD ductilities are similar to one another. The average r-value is only slightly

greater than one (r_{avg} = 1.13±0.10) with the highest value observed along the TD and the lowest along RD. It is also insightful to examine the in-plane anisotropy, Δr, previously defined [e.g., 17] as

$$\Delta r = \tfrac{1}{2}\left(r_{RD} + r_{TD} - 2r_{45}\right). \quad (4)$$

However, this parameter was devised to relate to earring behavior during deep drawing of cubic metal sheets. In the present work, it is useful to derive a second anisotropy denoted Δr_2,

$$\Delta r_2 = r_{\max} - r_{\min}, \quad (5)$$

which is simply the magnitude of the variation in r-value as a function orientation within the plane of the sheet. By this measure, it is shown that the conventional alloy has higher in-plane anisotropy than ZK10, which is in turn higher than that of the RE-containing alloys (Table 4.) Alloy ZE10 exhibits the most isotropic response in terms of either r_{avg} or Δr.

The basic property trends with alloying content are as follows. The yield strengths of alloy ZEK100 are slightly higher than ZE10, as are the elongations-to-failure. These are most likely a result of the finer grain size of the zirconium containing alloy, ZEK, since the texture, solute and precipitate content are similar. The strengths of alloy ZEK410 are even higher, which corresponds to the higher zinc content. Unfortunately, there is a commensurate decrease in ductility associated with the higher Zn content as well. Curiously, the strengths of alloy ZW41 are as low or lower than the alloys based on 1 or 2 wt% Zn. Additionally, the ductility of alloy ZW41 is nearly as high as ZEK100. While yttrium and cerium-rich mischmetal additions have a similar effect upon the texture (Fig. 3), the impact upon the mechanical properties is quite distinct. If strength is the primary objective, Ce would be preferred, but Y seems to promote better ductility.

Discussion

Texture:

Typical textures of magnesium sheets are reported in a number of related studies dealing mostly with common sheet alloy AZ31 [e.g., 18]. In any of these cases, a "basal" texture similar to that observed for alloy ZM21 in the present study is presented. While ZM21 is not a common commercial sheet alloy, this alloy has been used historically to make extruded tubes for manufacturing bicycle frames, for instance [19]. Thus, regardless of whether the primary alloying element is Al or Zn, the typical magnesium alloy sheet texture is obtained.

Styczynski et al. [18] have shown that polycrystal plasticity simulations which incorporate a combination of basal <*a*>, prismatic <*a*>, and pyramidal <*c*+*a*> slip along with {10.2} tensile twinning will predict this type of basal texture during cold rolling, including the symmetrical split of the peak basal pole intensity towards the RD as shown for alloy ZM21 in Figs. 3 & 4. Both basal slip and tensile twinning promote formation of the texture component with basal poles parallel to the ND. Especially twinning contributes to a rapid reorientation of grains during deformation [20, 21] such that the observed basal-type textures can be produced after only small reductions in thickness. Agnew et al. [22] stressed the significant role that <c+a> slip can have in rotating the basal poles from the ND direction toward the RD, to form the symmetric peaks described above and shown in Fig. 3. Alternatively, {10.1} compression twinning followed by {10.2} re-twinning has been hypothesized as a mechanism to promote this splitting of the basal poles toward the RD [23].

Warm rolling textures are also influenced by dynamic and/or static recrystallization. Typically, the recrystallization textures of magnesium alloys are qualitatively very similar to the deformation texture described above but quantitatively slightly weaker [e.g., 24, 25]. However, as mentioned above, although it has recently been shown that even though highly alloyed WE53 (Mg-5 wt% Y, 3wt%Nd) exhibits a rather typical magnesium sheet texture after warm plane strain compression [9], the texture becomes essentially random after a high

temperature recrystallization anneal [9]. Thus, the search for an explanation for the texture randomizing effect of RE/Y additions can be focused primarily on the recrystallization behavior. The crystallographic texture which results from recrystallization depends of the orientation of the nuclei on one hand and on any selective nature of the growth process on the other hand. In magnesium alloys, at least four nucleation mechanisms have been proposed.

i) *Grain boundary nucleation* of new grains seems to occur due to significant deformation in the "mantle" near the grain boundaries [26] accommodated by non-basal slip mechanisms. Thus, new grains are formed adjacent to the original grain boundaries leading to a kind of necklace-type microstructure. This mechanism does not lead to significant alteration of the original deformation texture in Mg [27].

ii) *Subgrain boundary motion* leads to coalescence of low angle boundaries and formation of increasingly high angle boundaries. This mechanism is promoted by the activity of non-basal slip [28], yet, like the grain boundary nucleation concept above it is not expected to strongly alter the deformation texture.

iii) There have been a variety of *shear band types* proposed as nucleation sites in magnesium alloys, including operation of basal slip in poorly oriented grains that leads to *kink band* formation, *linking of grain boundary deformation zones* referred to above [28], and *deformation twinning* itself [29]. Each of these band types can have basal planes nearly parallel to the shear plane and lead to some weakening of the overall basal texture in sheet material.

iv) Finally, particles can increase the driving force for recrystallization and act as nucleation sites by generating local inhomogeneties in the strain energy and orientation [8]. This can lead to *particle stimulated nucleation (PSN)* which provides more randomly oriented nuclei and results in weaker recrystallization textures. It has been proposed that nucleation occurs more frequently at particles

(PSN) in alloy WE43 than in conventional magnesium alloys, such as the most common sheet alloy AZ31 [11].

In all the RE/Y alloys presented in this study, the textures are clearly distinct from the conventional basal texture described for alloys AZ31 and ZM21. The textures have a significantly broader distribution of basal poles toward the TD, as compared to the RD, but so does non-RE-containing alloy ZK10. Additionally, the textures of the RE-containing alloys are weaker than those typically reported for AZ31 or ZM21, particularly if one considers the intensity of basal poles aligned parallel to the ND. There is only a slight compositional difference between alloys ZK10 and ZEK100 (notably, 0.17 wt% Ce-rich mischmetal) yet the texture of alloy ZEK100 is much weaker than that of ZK10. The texture of ZE10 is essentially the same as that of ZEK100; thus, it is concluded that the Zr content does not strongly alter the texture evolution.

The alloys with the highest alloy content had the weakest textures. Obviously, the more highly alloyed sheets have more particles (Fig. 1 and 2). Thus, the present results at first glance appear to lend some support to the notion that the texture randomizing effect of RE/Y additions is connected with the PSN mechanism described above. However, the most striking difference in the alloy textures is between ZM21 (which contains a significant particle distribution) and all the rest (including alloys ZK10 and ZE10, which have very few particles.) It is further noted that an increase of the Mn (i.e., particle) content in AZ31 does not lead to changes in the sheet texture [30]. This raises the question of why alloys containing RE/Y would be more inclined to exhibit PSN. Perhaps there is a distinction in the nature of the particles. However, recent data from binary alloy Mg 1wt% Y showed a significant texture randomizing effect upon recrystallization annealing, even though there are expected to be very few particles in this alloy, which suggests that second phase particles may not be necessary at all [5].

Alternatively, it is hypothesized that the observed texture modification may be more closely related to the nature of the solid solution alloy matrix. Notice that the texture-type qualitatively correlates with solute content. Even though alloy ZM21 has higher total alloy content than ZK10, the Zn solute content is expected to be lower, due to second phases which form [17]. This distinction in zinc solute appears to promote the splitting of the basal poles away from the ND toward the RD. Perhaps there is an additional propensity for a shear banding type deformation mechanism in the ZK and ZE alloys, as postulated long ago for dilute RE alloys [24]. One may argue that the higher (4 wt%) Zn alloys do not have higher solute content because the solid solubility for Zn at room temperature appears to be less than 1 wt%. However, the solubility at the working and annealing temperatures of interest (200-400ºC are in the range of 2 wt%. Further study will be required to determine the exact connections between RE/Y additions and the texture randomizing phenomenon. However, it is speculated that the reason RE elements strongly influence the recrystallization behavior of magnesium alloys is the same reason they affect the creep behavior, i.e., they are large atoms that are slow diffusers. Solute drag is known to distinctly influence the both the grain boundary mobility of different grain boundary orientation [31], specifically, and the recrystallization kinetics [32], in general.

Anisotropy:

The plastic anisotropy trends observed for the RE/Y containing alloys are opposite to those observed in the common alloy, AZ31, sheets [16]. We observe higher yield stresses and r-values along the RD than the TD in the RE/Y alloys. It has been reported many times that the TD is stronger than the RD in AZ31, and that the r-values are higher along the TD than the RD [16]. This behaviour has been related to the crystallographic texture which has greater spread of the basal poles toward the RD than the TD. Quantitative predictions of these properties are possible using polycrystal plasticity simulation, given the initial texture as input

and the single crystal plastic response, as characterized by the critical resolved shear stresses and hardening behaviours of the individual slip and twinning mechanisms. One advantage of this procedure is that the macroscopically observed behaviour may be linked to the grain-level mechanisms that are responsible in an efficient fashion, even for cases where single crystal growth is impossible. The value of polycrystal modelling has already been mentioned above in the context of simulating texture evolution.

The polycrystal plasticity approach employed in the present study is well-described in a paper by Lebensohn and Tomé [33]. The application of this approach to modeling the behavior of magnesium alloys is reviewed in Agnew and Duygulu [3]. The details of the twinning model employed and its application to a magnesium alloy are described by Tomé et al. [34] and Jain and Agnew [35], respectively. In brief, the orientation distribution is calculated from experimental pole figures using the direct method of Williams-Imhoff-Matthis-Vinel (WIMV) described by Kallend [36] and then discretized on a 10x10x10º grid of Euler space using Bunge's convention (φ_1, Φ, φ_2). This results in an ensemble of ~2000 orientations (grains) with the proper volume fraction ascribed to them in order to reproduce the experimentally observed texture.

The behavior of individual crystals of a given orientation is modeled using a viscoplastic crystal plasticity formulation described in [34]. The free parameters of the model are the crystal resolved shear stresses (CRSSs) and the hardening behaviors of the individual slip and twinning mechanisms. These are modeled using a Voce hardening rule:

$$\tau^s = \tau_0^s + \left(\tau_1^s + \theta_1^s \Gamma\right)\left\{1 - \exp\left(-\frac{\theta_0^s \Gamma}{\tau_1^s}\right)\right\} \tag{6}$$

where τ^s and θ^s values are the CRSS and strain hardening parameters of the s^{th} slip system respectively, and Γ is the accumulated shear strain. No latent hardening between slip or twinning systems was invoked during these simulations in order to keep the number of

adjustable parameters to a minimum. Further, it has been found that the behavior of the main twinning mode, {10.2} tensile twinning, is well-modeled as not hardening at all [36].

As an initial guess, the best-fit parameters for the room temperature mechanical behavior of AZ31 were utilized (see Table 5). Using the initial texture of ZW41 and these parameters, all the main features of the anisotropy are predicted. Namely, the RD tensile behavior is harder and exhibits a higher r-value than the TD tensile behavior. This indicates that the main features of the mechanical response are not primarily due to a change in the relative slip system strings, rather they are due to the unique crystallographic texture observed in these alloys. However, the predicted values of the r-values are too low and the hardening behaviors do not quantitatively match the experimental data using deformation mechanism parameters fit to the behavior of alloy AZ31.

In order to better fit the experimental data, the parameters which govern the individual deformation modes were altered from those in Table 4, to those presented in Table 5. The requirement for the model to simultaneously predict the experimentally observed r-values and flow curves obtained from the RD, TD and 45º oriented tensile samples serves to highly constrain the selection of model parameters. Most notably, the CRSS for basal <a> slip was increased relative to the other slip systems. This is an important finding for two reasons: i) the relative strengths of the slip systems determines their relative activities, which in-turn determines the anisotropy of the textured metal; and ii) it is consistent with previous experimental observations of solid solution alloys [37, 38, 39, 40], in general, and RE-containing alloys [41, 42], in particular, which indicated an increased density of non-basal dislocations.

At a detailed level, it was found that increased activity (decreased relative strength) of the non-basal <a> slip modes (prismatic {10.0} or pyramidal {10.1}) leads to an increase in the r-values of all three test directions. Using this approach, the average r-value (Eq. 3) from the three testing directions can be brought close to that observed experimentally, but the range (or

Δr parameter of Eq. 4) is still too high. This indicates that the individual crystals are still too anisotropic and a mechanism capable of accommodating c-axis compression, such as <c+a> slip, is required. Increasing the activity of <c+a> slip enables excellent agreement between the predicted and measured r-values to be obtained (Fig. 6b). It is noted that another c-axis compression mechanism would have a similar effect on the simulation results, whether it be a {10.1} compression twinning mechanism or kink banding. In order to determine which specific c-axis compression mechanism is responsible will require additional research.

The discussion above focuses on fitting the observed r-values because the flow curves are similarly well-modeled by a range of parameter values. Thus, the more discriminating test of the model is the correct prediction of r-values[*]. However, the flow curves themselves are revealing (Fig. 6a). Notice that the RD tensile test data exhibits parabolic hardening typical of slip-dominated deformation. Conversely, the TD flow curve exhibits essentially linear hardening. It is important to reiterate that a single set of model parameters is used to simulate the response in all of the tested directions. Thus, the polycrystal modeling approach enables connections to be made between the macroscopic mechanical response with the activity of specific deformation mechanisms.

For example, Figure 6c shows that the linear hardening during tension along the TD is primarily due to a combination of basal <a> slip and tensile twinning. Tensile twinning is favored in these RE-containing alloys during the TD tensile tests because there is a non-negligible volume fraction of grains with c-axes close to the TD (Fig. 3). The observed linear hardening is intermediate to the parabolic hardening of slip-dominated deformation and the sigmoidal (S-shaped) hardening observed for twin-dominated deformation, which occurs during in-plane compression of magnesium sheets [e.g., 36] or compression along the extrusion axis [43]. The crystallographic reorientation that occurs during tensile twinning

[*] For more details of the behavior and modeling of alloy ZW41, including measurements of the behavior in the temperature range of interest to warm forming, the reader is directed to a companion paper by Agnew and Chiu, in preparation for Inter. J. Plasticity [**Fehler! Textmarke nicht definiert.**].

generally places grains in a harder orientation with respect to continued slip or twinning, resulting in an increased macroscopic hardening rate. Barnett has previously noted that this type of linear hardening is due to a synergy between slip and twin accommodated flow in the discussion of transverse direction tensile testing of extruded bars, and further commented that such hardening leads to improved resistance to plastic instability according to Considére's criterion [44]. Indeed, the texture of the RE-containing alloy sheets approaches that of magnesium alloy extrusions, which have their c-axes perpendicular to the extrusion direction. Further, the ductility of the RE-containing alloys is highest along the TD or 45º directions, which exhibit an improved hardening response in comparison to the RD. Thus, the objective of producing improved hardening behavior and resistance to plastic instability can be accomplished via randomization of the texture.

Conclusions

Wrought magnesium alloys typically exhibit strong basal textures with only slight variations between them, and it has only recently been reported that alloys containing rare earth elements and/or yttrium (RE/Y) can develop more random textures. In this study, it is hypothesized that soluble zinc and rare earth additions (Ce or Y) are responsible for the modification of the rolling texture of alloys ZK10, ZE10, ZEK100, ZEK410 and ZW41 from the conventional texture observed in alloys AZ31 and ZM21. The basal pole intensity aligned with the sheet normal direction is low, rather than high, in all the high zinc solute alloys. Instead, the strongest basal intensities are tilted ~20º towards the rolling directions. The addition of rare earth elements leads to a weakening of the texture. Other studies link this latter result to distinct recrystallization behaviour of these alloys and further research is required to elucidate the specific mechanism(s) which are responsible.

Because the spread of the basal poles is greater toward the TD than the RD in the RE-containing alloys, the flow stresses are lower along the TD than the RD. Grains with c-axes

tilted away from the sheet ND toward the tensile axis are more favourably oriented for basal slip and tensile twinning, the soft deformation mechanisms in magnesium alloys. The significant activity of tensile twinning during TD tensile testing leads to linear hardening behaviour that promotes desirable plastic stability against necking.

Finally, a reduced planar anisotropy ($r \sim 1$) is observed, in comparison to conventional alloys that have higher r-values, This too is related to the weaker textures which have a larger volume fraction of grains oriented favourably to accommodate in-plane tensile deformation by basal slip and twinning, which promote sheet thinning. Mg sheets with lower r-values promise to have improved forming behaviour under straining conditions which call for thinning of the sheet (i.e., stretching), a problematic strain path for current Mg alloys.

Acknowledgements

The authors are grateful for rolling trials performed by Dr. Lothar Löchte at Hydro Aluminium Deutschland GmbH and Ms. Kerstin Nestler at GKSS as well as mechanical property measurements performed on alloy ZW41 by Mr. William Chiu at the University of Virginia. The National Science Foundation (Grant Number DMR-0603066)_and Deutsche Forschungsgemeinschaft (Grant Number LE 1395/3-1) World Materials Network financially support this collaboration. SRA and JWS are also grateful for financial support of Oak Ridge National Laboratory through a Joint Faculty Appointment and a National Science Foundation Collaborative Research Grant Number DMI-0322917.

References

1. Friedrich H, Schumann S, J. Mater. Proc. Tech. 117 (2001) 276 – 281.
2. Mann G, Griffiths JR, and Cáceres CH, J. Alloys Comp., 378 (2004) 188-191.
3. Agnew SR and Duygulu O, Inter. J. Plasticity, 21 (2005) 1161–1193.
4. Hosford WF and Caddell RM, in Metal Forming (PTR Prentice Hall: Upper Saddle River, NJ: 1993) 68-79.
5. Agnew SR, Senn JW, and Horton JA, JOM, 58 (2006) 62 – 69.

6. Luo AA and Sachdev AK, in: Luo AA, Neelameggham and Beals RS, Magnesium Technology 2006 (TMS, Warrendale 2006), 333 – 339.
7. Yukutake E, Kaneko J, and Sugamata M, Trans. JIM, 44 (2003) 452-457.
8. Ball EA and Prangnell PB, Scripta Metall. Mater., 31 (1994) 111-116.
9. Senn JW and Agnew SR, In: Proc. Magnesium Technology in the Global Age, Montreal, Canada (2006) in press.
10. Lorimer GW, Mackenzie LWF, Humphreys FJ, and Wilks T, Mater. Sci. Forum, 467-470 (2004) 477-482.
11. Lorimer GW, Mackenzie LWF, Humphreys FJ, and Wilks T, Mater. Sci. Forum, 488-489 (2005) 99-102.
12. Humphreys FJ, Acta metal. 25 (1977) 1323 – 1344.
13. Chiu WV and Agnew SR, in preparation for the Inter. J. Plasticity.
14. Kree V, Bohlen J, Letzig D, Kainer KU, Pract. Metallography 41 (2004) 233.
15 Kaiser F, Bohlen J, Letzig D, and Kainer KU, Mat. Sci. Forum. 419-422 (2003) 315-320.
16. Villars P, Prince A, Okamoto H, Handbook of Ternary Alloy Phase Diagrams, Materials Park, Ohio, ASM International, 1995
17. Hosford WF and Caddel RM, Metal Forming: Mechanics and Metallurgy, 2nd Ed.(Prentice Hall: Upper Saddle River, NJ, USA: 1993) 298-301.
18. Styczynski A, Hartig Ch, Bohlen J, Letzig D, Scripta Mater. 50 (2004) 943–947
19. Deetz J, JOM 57 /5 (2005) 50-53.
20. Davies CHJ, Yi S, Bohlen J, Kainer KU, Brokmeier HG, Mat. Sci. Forum 495 – 497 (2005) 1633
21. Brown DW, Agnew SR, Bourke MAM, Holden TM, Vogel SC and Tomé CN, Mat. Sci. Eng A 399 (2005) 1-12.
22. Agnew SR, Tomé CN, and Yoo MH, Acta Mater. 49 (2001) 4277-4289.
23. Couling SL, Pashak JF, and Sturkey L, Trans. ASM, 51 (1959) 94-107.
24. Gehrmann R and Gottstein G, in: Szpunar JA ed., Proc. 12th Inter. Conf. Textures Mater. (NRC-CNRC Research Press: Ottawa, Canada: 1999) 665-670.
25. Nadella RK, Samajdar I, and Gottstein G, in: Kainer KU Ed., Magnesium Alloys and their Applications (DGM Wiley-VCH: Weinheim, Germany: 2003) 1052-1057.
26. Ashby MF, Phil. Mag., 21 (1970) 399-424.
27. Ion SE, Humphreys FJ, and White SH, Acta Metall. 30 (1982) 1909-1919.
28. Galiyev A, Kaibyshev R, and Gottstein G, Acta Mater., 49 (2001) 1199-1207.
29. Myshlyaev MM, McQueen HJ, Mwembela A, and Konopleva E, Mat. Sci. Eng. A, A337 (2002) 121-133.
30. Laser T, Nürnberg MR, Janz A, Hartig Ch, Letzig D, Schmid-Fetzer R, Bormann R, Acta Mater. 54 (2006) 3033 – 3041.
31. Humfreys FJ and Hatherly M, Recrystallization and Related Annealing Phenomena (Elsevier: Oxford: 1995) 102-111.
32 . Lucke K and Deter K, Acta Metall., 5 (1957) 628-637.
33. Lebensohn RA and Tomé CN, Mat. Sci. Eng. A 175 (1994) 71 – 82.
34. Tomé CN, Lebensohn RA, Kocks UF, Acta Mater. 39 (1991) 2667-2680.
35. Jain A and Agnew SR, Mat. Sci. Eng. A (2006) in press.
36. Kallend JS, in: Kocks UF, Tomé CN and Wenk HR, Texture and Anisotropy (Cambridge University Press, Cambridge MA: 1998) 102 - 125.
37. Akhtar A and Teghtsoonian E, Acta Mater., 17 (1969) 1339-1349.
38. Akhtar A and Teghtsoonian E, Acta Mater., 17 (1969) 1350-1356.
39. Urakami A and Fine ME, Proc. First Inter. Conf. Mech. Behavior Mater., (Kyoto: 1971) pp. 87-96.
40. Cáceres CH and Blake A, Phys. Stat. Sol. 194 (2002) 147-158.

41. Suzuki M, Sato H, Maruyama K, and Oikawa H, Mat. Sci. Eng. A, A252 (1998) 248-255.
42. Suzuki M, Sato H, Maruyama K, and Oikawa H, Mater. Sci. Eng. A, A319-321 (2001) 751-755.
43. Barnett MR, Keshavarz Z, Beer AG, Atwell D, Acta Mater. 52 (2004) 5093-5103.
44. Barnett MR, presented in the Magnesium Technology 2006 Symposium, San Antonio, TX, March (2006).

Table 1: Properties and composition of sheets used in this study (Mg balance)

Alloy	Final gage [mm]	Average Grain Size [μm]	Alloy Composition [wt.%]						
			Zn	Mn	Ce	Nd	La	Y	Zr
ZM21	1.0	14	2.1	0.9	-	-	-	-	-
ZK10	1.0	9	1.0	-	-	-	-	-	0.3
ZE10	1.1	18	1.3	-	0.1	-	-	-	-
ZEK100	1.4	9	1.3	-	0.2	-	0.1	-	0.5
ZEK410	1.1	10	4.3	-	0.7	0.2	0.2	-	0.5
ZW41	1.0	15	4.0	-	-	-	-	0.7	-

Table 2: EDS analysis of particles as shown in SEM images in Figs. 2a- f (all values in wt. %), [1)] 6.1 Nd, 0.9 Si, [2)] 2.0 Sr

Alloy	Particle	Mg	Zn	Mn	Ce	La	Y	Zr	Others
ZM21	I	79.0	3.0	18.0	-	-	-	-	-
	II	80.2	1.4	18.4	-	-	-	-	-
	III	93.4	3.9	2.7	-	-	-	-	-
	IV	93.5	2.1	4.4	-	-	-	-	-
ZK10	I	86.9	1.1	-	-	-	-	12.0	-
	II	95.0	1.1	-	-	-	-	3.9	-
	III	77.6	0.9	-	-	-	-	21.5	-
ZE10	I	78.2	2.2	-	9.3	3.4	-	-	7.0[1)]
	II	94.0	3.4	-	1.6	1.1	-	-	-
	III	92.1	5.2	-	1.6	1.1	-	-	-
ZEK100	I	66.8	13.1	-	12.9	7.3	-	-	-
	II	58.5	16.3	-	15.0	10.3	-	-	-
	III	89.6	5.1	-	3.1	1.6	-	-	-
	IV	58.4	18.3	-	16.1	7.2	-	-	-
	V	92.4	4.1	-	-	-	-	3.6	-
	VI	95.9	2.3	-	-	-	-	1.9	-
ZEK410	I	5.7	32.2	-	-	-	-	60.2	2.0[2)]
	II	55.2	26.7	-	12.6	5.5	-	-	-
	III	93.4	5.6	-	-	-	-	1.1	-
	IV	65.5	20.2	-	10.0	4.4	-	-	-
	V	95.6	3.9	-	-	-	-	0.5	-
	VI	90.7	5.8	-	2.3	1.2	-	-	-
	VII	43.7	34.7	-	15.8	5.8	-	-	-
ZW41	I	21.7	1.0	-	-	-	77.3	-	-
	II	82.4	2.7	-	-	-	14.9	-	-
	III	90.2	7.1	-	-	-	2.7	-	-
	IV	89.6	8.2	-	-	-	2.2	-	-
	V	90.5	7.3	-	-	-	2.2	-	-
	VI	84.7	10.8	-	-	-	4.5	-	-

Table 3: Mechanical sheet properties (TYS – tensile yield stress, UTS – ultimate tensile stress)

Alloy	Orientation	TYS MPa	UTS MPa	uniform elongation %	elongation %
ZM21	RD	127	236	18.4	24.3
	45°	133	228	16.3	21.2
	TD	144	235	14.6	18.1
ZK10	RD	194	254	10.0	15.6
	45°	206	256	12.1	23.1
	TD	226	272	11.2	22.5
ZE10	RD	191	216	7.7	19.8
	45°	154	216	18.5	28.2
	TD	138	226	18.9	29.7
ZEK100	RD	203	234	7.1	23.7
	45°	163	231	15.3	39.3
	TD	154	241	15.7	31.9
ZEK410	RD	258	291	4.9	8.8
	45°	199	273	13.3	20.6
	TD	182	280	17.5	23.7
ZW41	RD	209	258	10.8	17.4
	45°	147	243	20.9	26.5
	TD	130	248	22.1	30.1

Table 4: Planar and in-plane anisotropy of magnesium sheets

Alloy	r_{RD}	r_{45}	r_{TD}	r_{avg}	Δr	Δr_2
ZM21	0.9	1.4	2.1	1.45	0.1	1,2
ZK10	0.9	1.2	1.3	1.15	-0.1	0.4
ZE10	0.9	1.0	0.9	0.95	0.1	0.1
ZEK100	0.9	1.3	1.2	1.18	-0.25	0.4
ZEK410	*1.3**	1.1	0.9	1.1	0	0.4
ZW41	0.9	1.1	0.7	0.95	-0.3	0.4

**italics*: value at maximum uniform strain 5%,

Table 5. Voce hardening parameters of the individual deformation mechanisms fit to the behavior of annealed magnesium alloy AZ31 sheet, after ref. [35]. All values are scaled relative to τ_0(basal) = 1.0, and must be multiplied by 24.5 MPa in order to match the experimental.

Deformation Mode	τ_0	τ_1	θ_0	θ_1
basal <***a***>	1.0	0.5	40	3.0
prism <***a***>	4.5	2.0	20	1.2
<***c+a***>	7.0	2.3	800	0
tension twin	1.6	0	0	0

Table 6. Voce hardening parameters of the individual deformation mechanisms fit to the behavior of annealed magnesium alloy ZW41 sheet. Again, all values are scaled relative to τ_0(basal) = 1.0, and must be multiplied by 29 MPa in order to match the experimental.

Deformation Mode	τ_0	τ_1	θ_0	θ_1
basal <***a***>	1.0	1.0	10	1.0
prism <***a***>	3.5	1.5	15	1.0
<***c+a***>	4.5	1.0	45	0
tension twin	1.0	0	0	0

a) ZM21

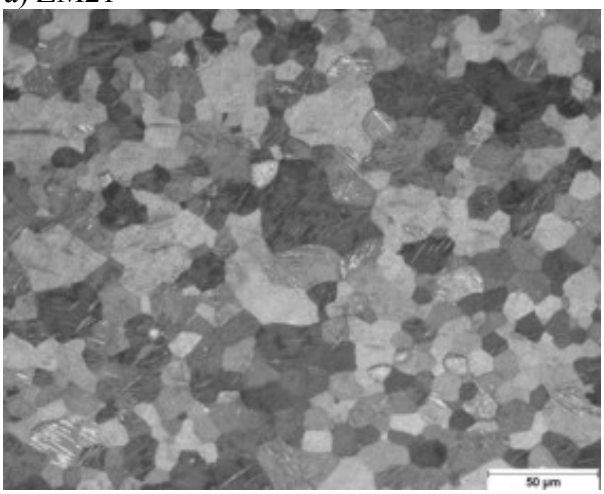

b) ZK10

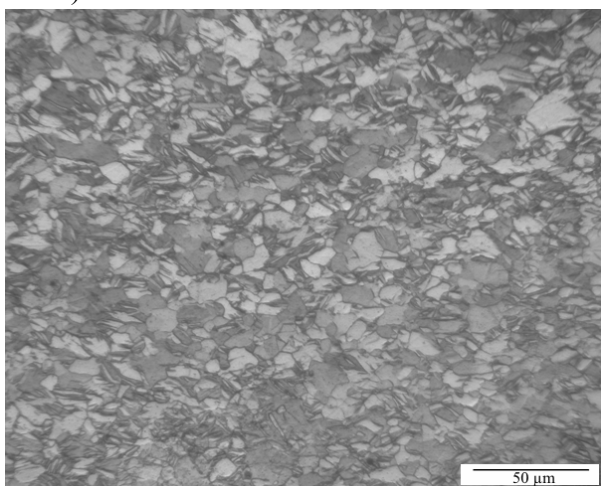

c) ZE10

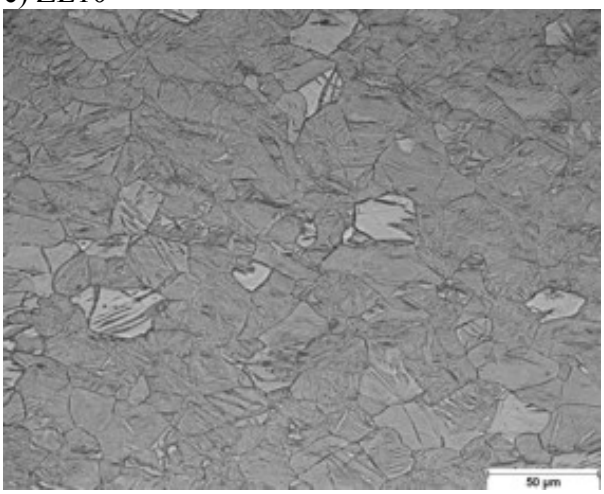

d) ZEK100

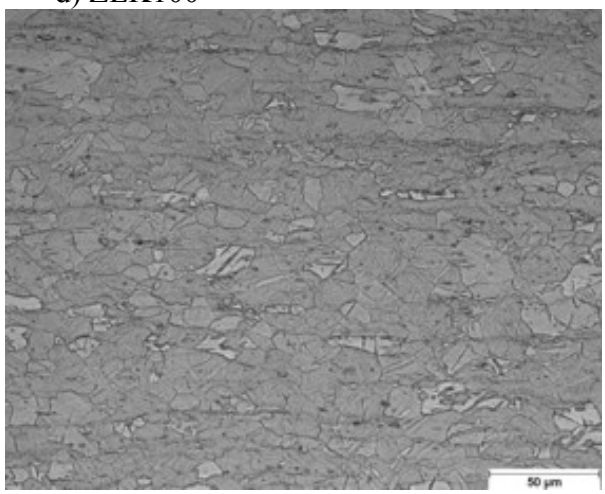

e) ZEK410

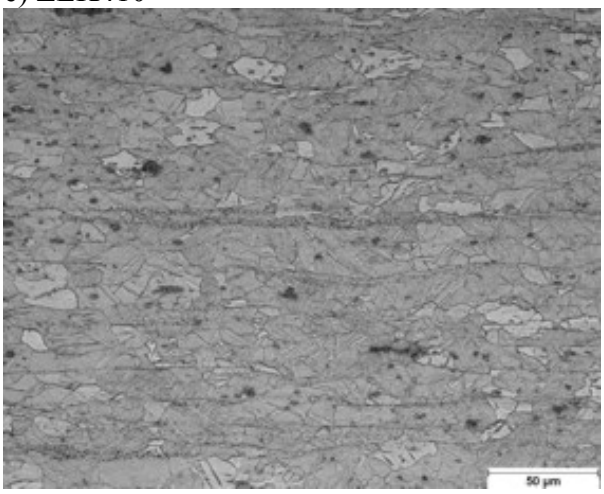

f) ZW41

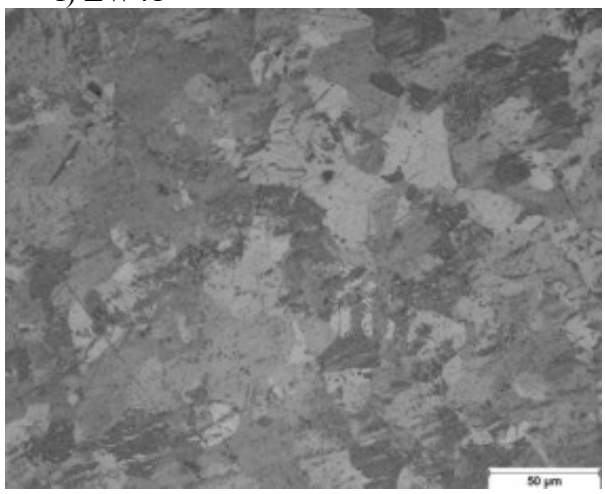

Figure 1: Sample micrographs of magnesium sheets (RD horizontal), a) ZM21, b) ZK10, c) ZE10, d) ZEK100, e) ZEK410, f) ZW41

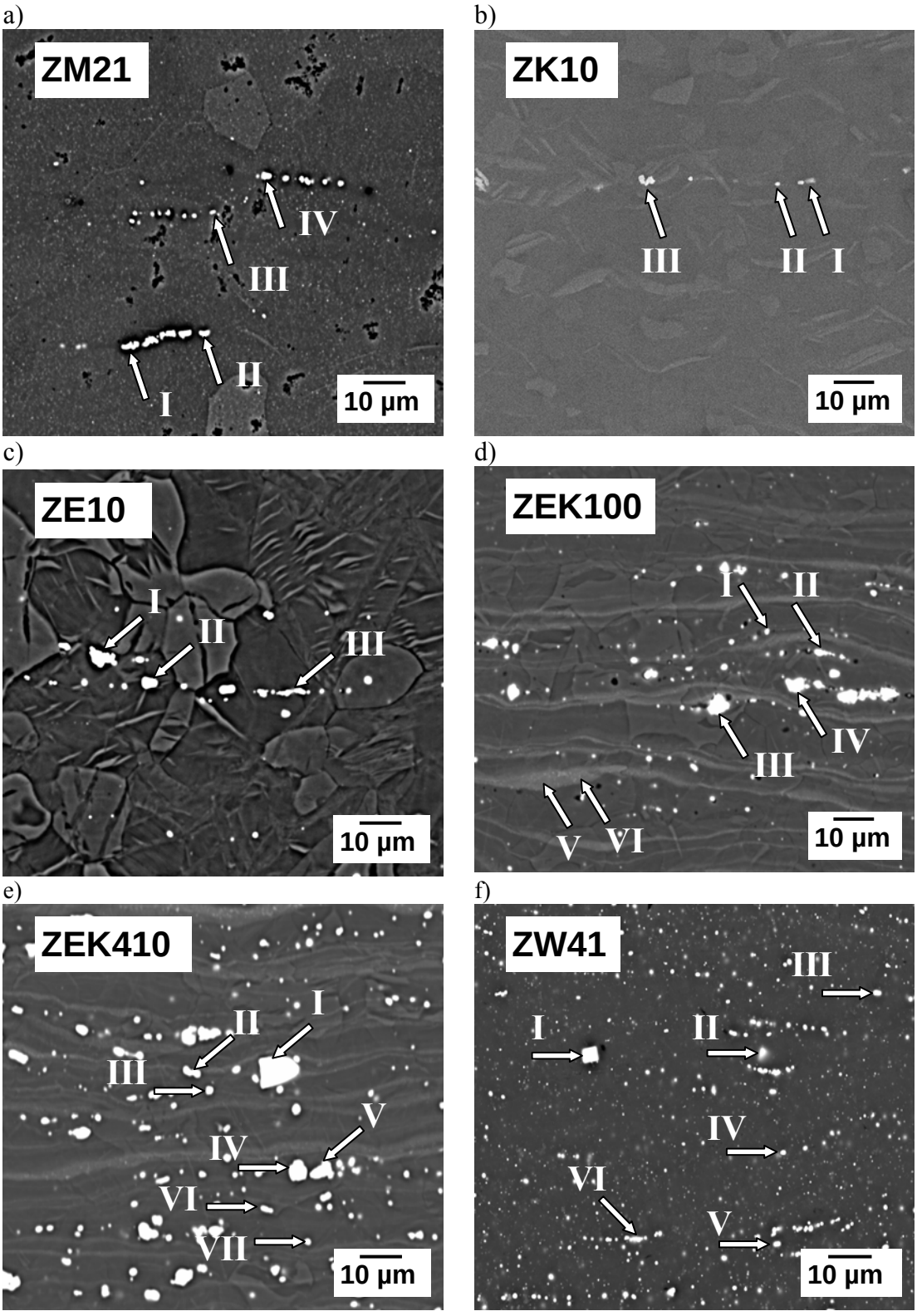

Figure 2: SEM images showing different particles in the microstructure of sheets. The composition of designated particles is collected in Table 1, a) ZM21, b) ZK10, c) ZE10, d) ZEK100, e) ZEK410, f) ZW41

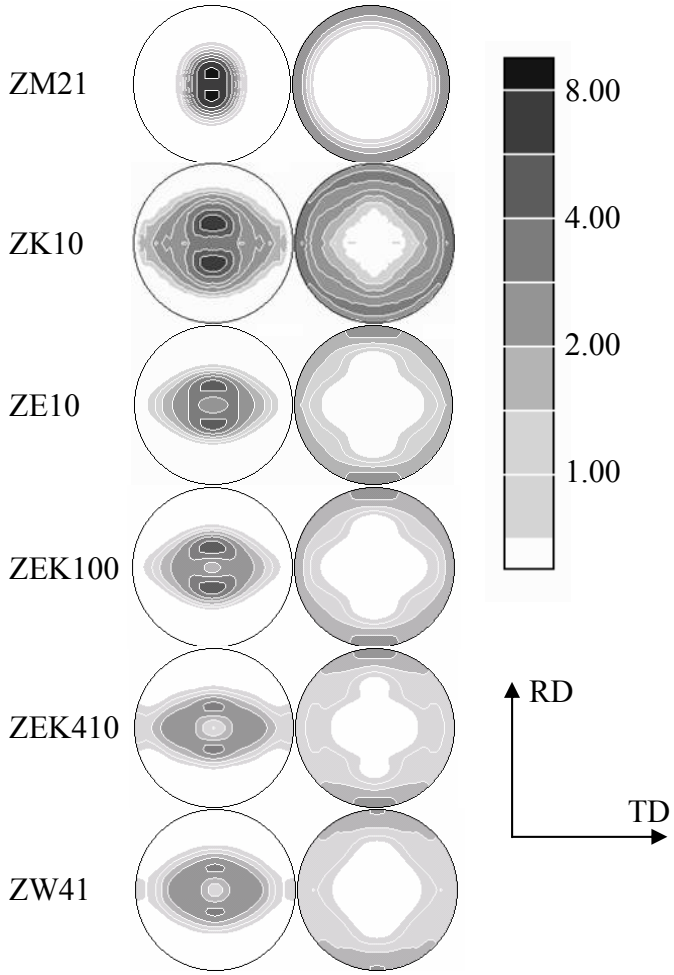

Figure 3: Equal area projection of texture measurements on rolled samples.

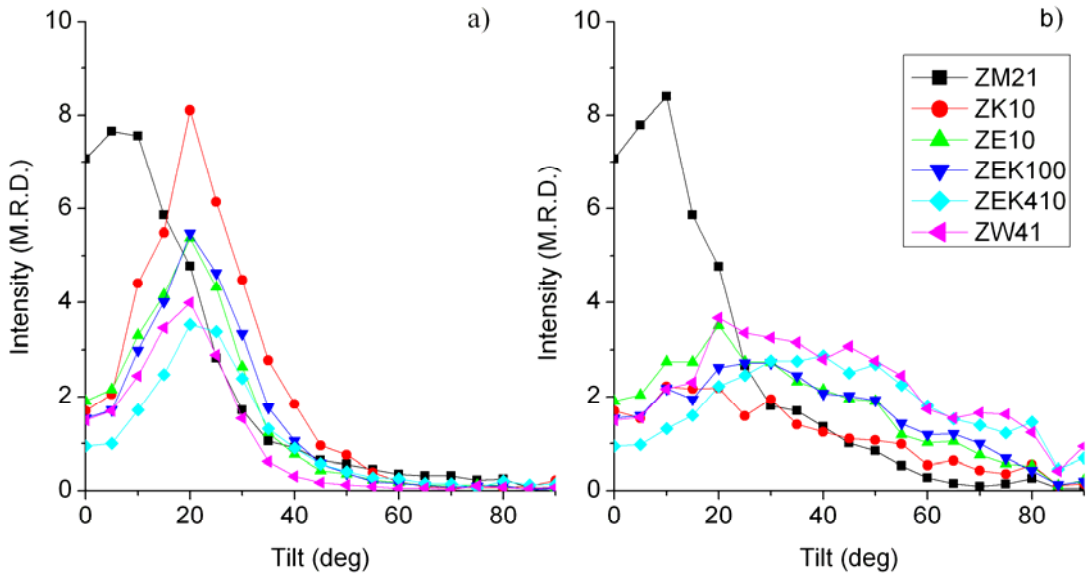

Figure 4. Texture comparison with the intensity (in multiples of a random distribution or M.R.D.) in the basal pole figures plotted as a function of tilt from the sheet normal direction toward the a) rolling or b) transverse direction.

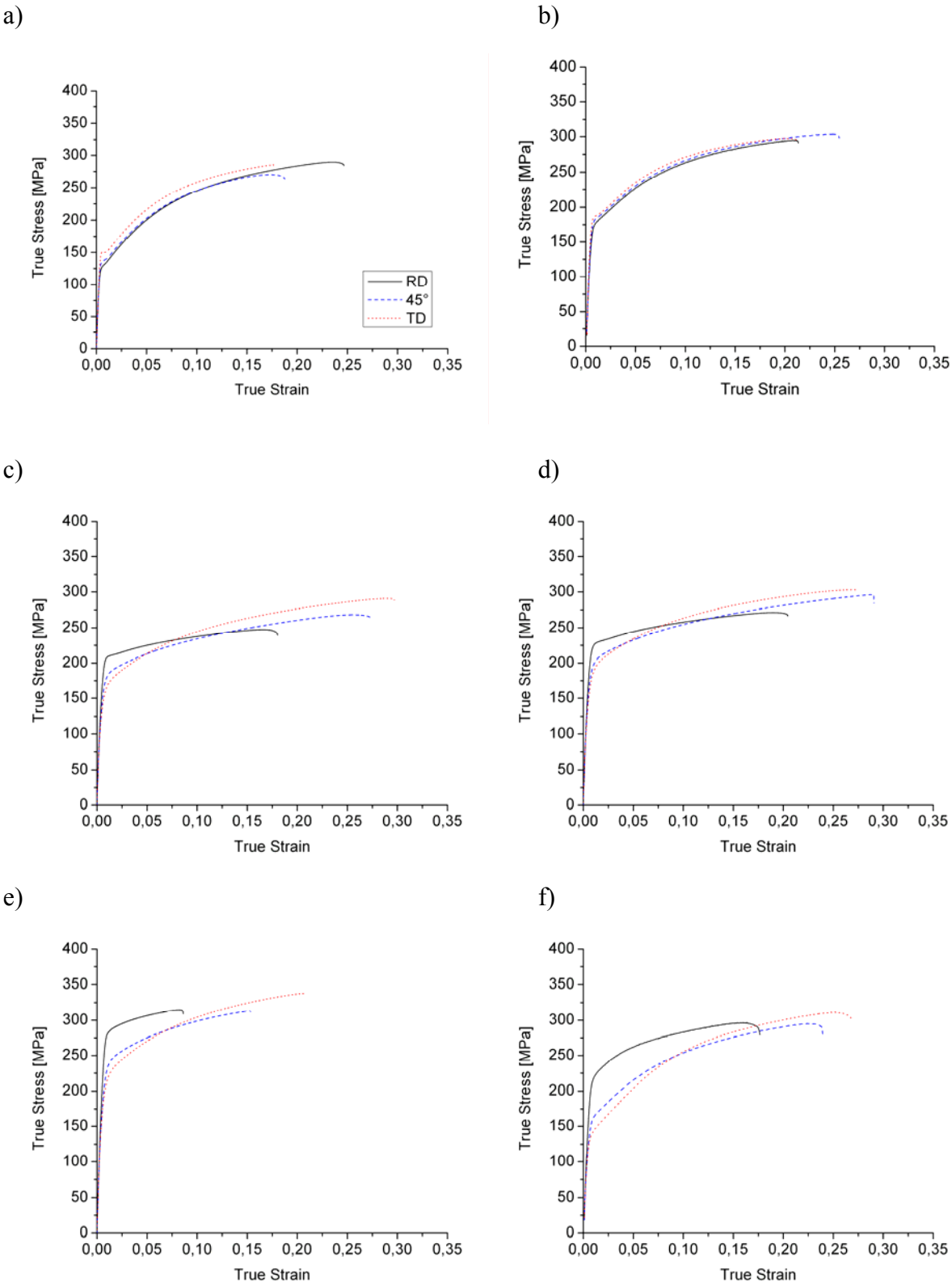

Fig. 5: True stress – true strain curves from tensile tests in three sheet orientations (RD, 45°, TD), a) ZM21, b) ZK10, c) ZE10, d) ZEK100, e) ZEK410, f) ZWK410

a)

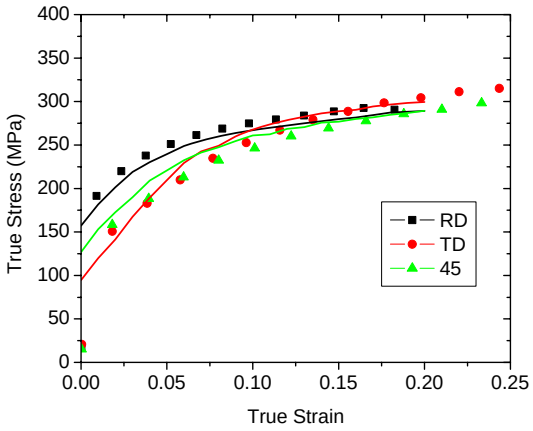

b)

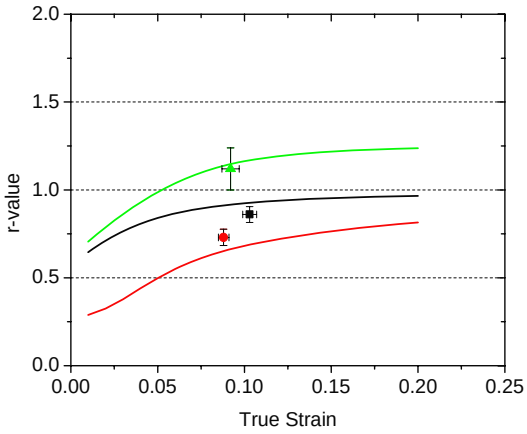

c)

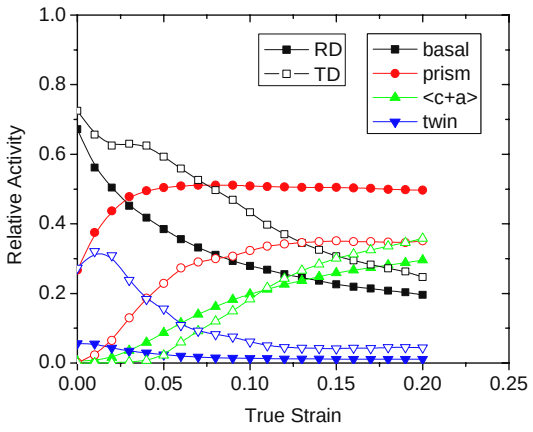

Figure 6. Comparison of experimental and simulated a) flow curves and b) r-values of annealed alloy ZW41, and c) the simulated activities of the deformation mechanisms during rolling and transverse direction tensile tests (45º direction data are intermediate.)